MATERIALS SCIENCE

Reconfigurable structure and tunable transport in synchronized active spinner materials

Koohee Han[1]*, Gašper Kokot[1,2]*, Shibananda Das[3,4]*, Roland G. Winkler[3], Gerhard Gompper[3], Alexey Snezhko[1]†

Ensembles of actuated colloids are excellent model systems to explore emergent out-of-equilibrium structures, complex collective dynamics, and design rules for the next generation materials. Here, we demonstrate that ferromagnetic microparticles suspended at an air-water interface and energized by an external rotating magnetic field spontaneously form dynamic ensembles of synchronized spinners in a certain range of the excitation field parameters. Each spinner generates strong hydrodynamic flows, and collective interactions of the multiple spinners promote a formation of dynamic lattices. On the basis of experiments and simulations, we reveal structural transitions from liquid to nearly crystalline states in this novel active spinner material and demonstrate that dynamic spinner lattices are reconfigurable, capable of self-healing behavior and that the transport of embedded inert cargo particles can be remotely tuned by the parameters of the external excitation field. Our findings provide insights into the behavior of active spinner materials with reconfigurable structural order and tunable functionalities.

INTRODUCTION

Ensembles of out-of-equilibrium particles are an important platform to unravel design rules for the next generation of reconfigurable materials due to their ability to self-organize (*1*–*3*). External energy influx provided by an electric or magnetic field has enabled assemblies of actuated particles to change their dynamic and collective response in a controlled manner by simply modulating excitation field parameters (*4*–*10*). In addition to their fundamental importance, these field-driven active systems are promising candidates for practical applications such as water purification and targeted drug delivery by tuning their transport properties on demand (*11*, *12*).

Most of the research so far has been focused on self-propelled particles exhibiting a wealth of self-organized phenomena ranging from dynamic chaining and clustering to flocking and active turbulence (*13*–*20*), while systems with activities originating from purely rotational motion of elementary units have been waiting their turn. One of the first realizations of dynamically assembling system of spinners has been demonstrated at the macroscopic level in a system of magnetized disks suspended at a liquid interface and powered by a rotating magnetic field. There, a same-wise rotation of particles lead to stable dynamically ordered phases similar to crystals (*21*). Recently, there have been increasing efforts to investigate colloidal systems with a rotational active motion by designing chiral active units (*22*–*27*) or enforcing local torques by external driving fields (*28*–*35*). Related simulation studies have predicted an intriguing collective dynamics in active spinner systems such as phase separation, lattice formation, and flow generation (*26*–*30*, *36*, *37*).

Approaches exploiting the dynamic self-assembly of colloidal particles provide a robust method for generating large ensembles of microscopic spinners (*23*, *33*, *38*). It has been demonstrated that an application of a uniaxial external magnetic field oscillating in-plane of the interface supporting ferromagnetic spherical particles can lead to multiple self-assembled spinners with a narrow size distribution (*23*, *38*). These magnetic self-assembled spinners with spontaneously selected chiralities yield an efficient interfacial mixing, facilitated by spinner-induced vortical hydrodynamic flows, and exhibit an active turbulence (*38*). The rate and corresponding scale of energy injection are tuned by the amplitude and frequency of the applied magnetic field.

However, these spinners, emerging via spontaneous breaking of the uniaxial symmetry of the external in-plane field, are not easy building blocks for a dynamic assembly due to the fact that they rotate in random directions and perpetually disintegrate and self-assemble (*38*). To gain a better control and tunability of the active spinner material, we present a system of synchronously corotating self-assembled spinners that are stable and efficiently coupled by the self-induced hydrodynamic flows.

Here, we report swarms of synchronized self-assembled spinners dynamically formed from ferromagnetic nickel (Ni) particles suspended at an air-water interface and energized by an in-plane rotating magnetic field. The magnetic field drives the dynamic self-assembly of the Ni particles into multiparticle linear chains of approximately equal length that remain synchronized with the rotation of the external field. The field frequency sets the characteristic size of the assembled spinners determined by a balance between magnetic and viscous torques exerted on a chain at a liquid interface (*23*, *39*). Self-assembled spinners locally inject vorticity into the liquid interface and generate strong hydrodynamic flows, leading to a set of collective dynamic phases. Transitions from a spinner liquid phase to stable two-dimensional (2D) dynamic crystalline lattices are observed with increasing spinner density (*36*). The phases are dynamic by nature and exist while the energy is injected into the system. This is in contrast to 2D colloidal crystals, where lattice elements are static and do not rely on hydrodynamic interactions for stability (*40*). We combine experiments and simulations to probe the structural and transport properties of these active spinner materials. We show the importance of the particle number density and the rotational field frequency for the structural transitions in the active spinner

[1]Materials Science Division, Argonne National Laboratory, Lemont, IL 60439, USA. [2]Northwestern Argonne Institute of Science and Engineering (NAISE), Engineering Science and Applied Mathematics, Northwestern University, Evanston, Illinois 60208, USA. [3]Institute of Complex Systems and Institute for Advanced Simulation, Forschungszentrum Jülich, 52425 Jülich, Germany. [4]Department of Chemistry, Columbia University, New York, NY 10027, USA.
*These authors contributed equally to this work.
†Corresponding author. Email: snezhko@anl.gov

system. We demonstrate that active spinner lattices exhibit self-healing behavior and reveal that the transport of inert particles facilitated by an active spinner ensemble in the dynamic spinner lattice states can be efficiently manipulated by the parameters of the external filed. Our findings provide insights into the properties of synthetic active spinner materials and yield tools for particle transport and manipulation at the microscale.

RESULTS AND DISCUSSION

Formation of self-assembled spinners and self-induced hydrodynamics flows

The process of dynamic self-assembly of spinners from ferromagnetic nickel particles suspended at an air-water interface starts by first applying a static magnetic field perpendicular to the liquid interface to disperse the suspended particles (Fig. 1A). Subsequently, the system is energized by an external rotating magnetic field applied in-plane with the interface ($\mathbf{H} = H_0(\sin(\omega t),\cos(\omega t),0)^T$, where H_0 is the field amplitude and $\omega = 2\pi f_H$ is the angular frequency controlled by the frequency of the excitation field (f_H) to drive the assembly of multiparticle linear chains (Fig. 1B). H_0 was fixed at 4 mT throughout the experiments unless otherwise stated. Once the chains were assembled, they kept rotating synchronously with the external magnetic field in a wide range (from 30 to 100 Hz) of the external field frequencies f_H used in the experiments. The self-assembly of spinners is a fully reversible process controlled by the parameters of the external field. The length of the particle chains changes in situ following the changes in the frequency of the field.

The length of an individual self-assembled spinner, L_S, is determined by a balance between magnetic and viscous torques exerted on the spinner (*39*, *41*) and can be tuned by f_H (see Fig. 1C and the Supplementary Materials). As the driving field frequency decreases the dipole-dipole attraction between rotating chains of ferromagnetic, particles becomes dominating and chains start to aggregate first into rotating clusters extending along the field direction and then further collapse into a single cluster. For our experimental conditions, the above process takes place at frequencies below 10 Hz. Control

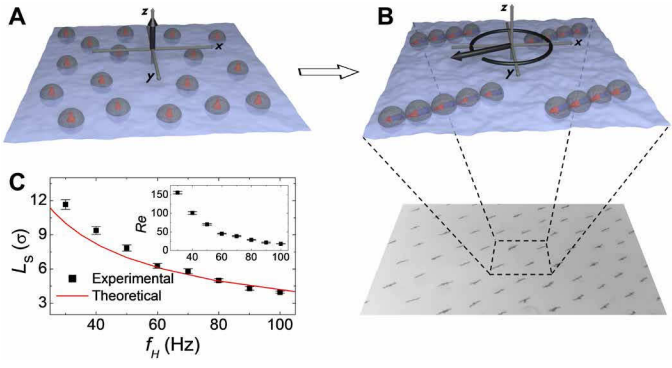

Fig. 1. Magnetic field–driven assembly of multiparticle spinners. (**A**) Schematics of a dispersed state of Ni particles under a static magnetic field along the *z* direction. (**B**) Assembly of spinners under influence of a rotating magnetic field applied in the *xy* plane (the bottom snapshot is a representative experimental image). (**C**) Spinner size as a function of field frequency f_H at $\rho = 0.006\ \sigma^{-2}$. The chain length, L_S, is normalized by the particle diameter, σ (90 μm). The solid line is a calculated theoretical curve (see the Supplementary Materials). Inset: Reynolds number, *Re*, of the spinners as a function of f_H.

over L_S has a direct impact on hydrodynamic behavior of the system assessed by the Reynolds number, *Re*, for an individual spinner, $Re = 2\pi f_H L_S^2/\nu$ (ν is the kinematic viscosity of the liquid). Our experimental system allows tuning of *Re* in the range from 30 to 150 (see inset of Fig. 1C).

An isolated spinner does not self-propel and keeps rotating at the same position without net displacement. In contrast, multiple spinners being advected by flows induced by neighboring spinners can move around and are able to self-organize into nearly lattices-like structures (see Fig. 2 and movie S1). The flows are the strongest around the sweep area of the rotating chains and decay with the distance from the spinners. The vorticity around the spinners coincides with the spinner rotation direction (Fig. 2B, red color) but transits to counterrotating flow in the large gaps between the spinners (Fig. 2, B and C). The latter follows from the flow field of the Stokes flow around a spherical (disk-like) particle of diameter L_S, which is given by

$$v(r) = \pi f_H L_S \left(\frac{L_S}{2r}\right)^{\delta-1} \quad (1)$$

in δ dimensions for distances *r* outside of the spinner area and in its vicinity (*38*). Calculation of the vorticity yields $\nabla \times \boldsymbol{v} \sim (2-\delta)/r^{\delta}$, which is negative for $\delta = 3$.

To get insights into the experiments and to elucidate the generic mechanisms governing the structure and collective dynamics in spinner ensembles, we perform simulations of rotating self-assembled spinners in 2D model systems. This raises the important issue of the relevance of the dimensionality of the flow field around the particles. Already, the flow field (and vorticity) depends on the spatial dimension, as seen in Eq. 1. For the interaction of pairs of spinning rotationally symmetric particles (discs) at finite Reynolds number *Re*, it has been argued that in 3D secondary flows dominate and make the interaction always repulsive (*42*), whereas in 2D a competition between hydrodynamic long-range attraction and short-range repulsion implies a preferred distance between particle pairs (*36*). The magnetic spinners in our experiments (and simulations) differ in two important aspects from the rotating discs in (*21*, *36*): (i) The magnetic attraction between the particles is strong enough for them to overcome the repulsion and to form chains, and (ii) the spinners are highly anisotropic, and therefore the flow field is varying periodically in time on shorter distances. This implies (i) that result for spinning disc should apply to our system at best qualitatively, if at all, and (ii) that dimensionality should play a role but may not substantially affect qualitative results, as hydrodynamic short-range repulsion of spinners is expected at finite Reynolds numbers in both 2D and 3D systems.

Structural order in synchronized spinners swarms

Large ensembles of the synchronized self-assembled spinners exhibit a tendency toward dynamic self-organization. The formation of lattices of spinners spanning nearly the whole air-water surface of the container has been observed in the experiments. To quantify the local ordering of the spinners, we calculated the hexagonal bond-orientational order parameter, ψ_6

$$\psi_6 = \frac{1}{N_b(m)} \sum_{n=1}^{N_b(m)} e^{6i\theta_{mn}} \quad (2)$$

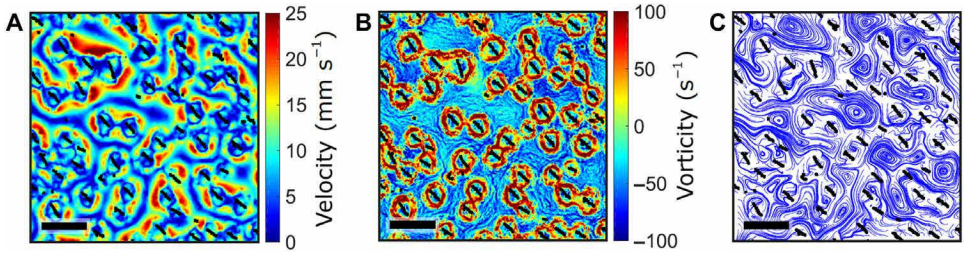

Fig. 2. Hydrodynamic flows generated by the synchronous spinners. (**A**) The flows velocity field as obtained from particle image velocimetry, (**B**) the local vorticity field, and (**C**) flows streamlines at f_H = 90 Hz and ρ = 0.0186 σ^{-2}. The spinners are shown in black as retrieved from the original microscopy image. Scale bars, 2 mm.

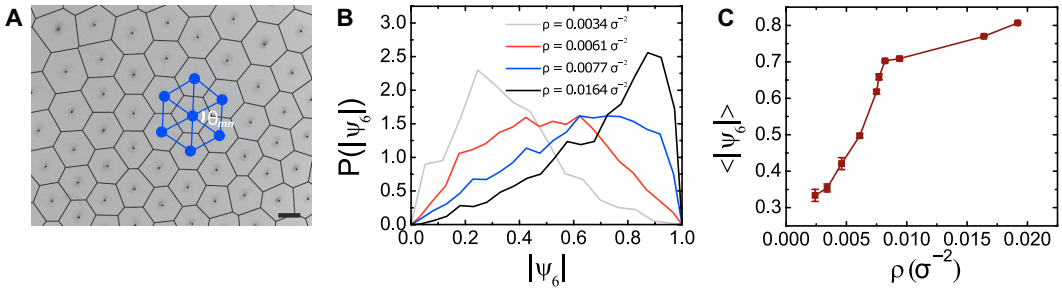

Fig. 3. The local ordering of the experimentally obtained spinner lattices. (**A**) A dynamic lattice formed from spinners at f_H = 45 Hz and ρ = 0.0164 σ^{-2}. Voronoi diagram is overlaid with the observed lattice. The spinners are blurred because of the long exposure time that enabled precise identification of the rotational axes for all spinners. Scale bar, 1 mm. (**B**) The probability distribution of the hexagonal bond-orientational order parameter $|\psi_6|$ in the spinner lattices at f_H = 45 Hz as a function of ρ. (**C**) The mean ψ_6 value of the spinner lattices illustrates the liquid-to-crystalline dynamic phase transition with the spinner density ρ.

Here, $N_b(m)$ is the number of nearest neighbors of the mth particle and θ_{mn} is the angle between some fixed axis and the line joining the mth and nth particle. The nearest neighbors for each spinner were determined by Voronoi construction (Fig. 3A) (*43*). Lattices with a perfect hexagonal order would result in $\psi_6 = 1$. For the dynamically organized spinner lattices, the degree of hexagonal ordering monotonically grew with the increase in the particle number density, ρ, as shown in Fig. 3B by the probability distribution function of $|\psi_6|$, obtained at a fixed frequency f_H = 45 Hz. Yet, the ordering is practically independent of the excitation frequency f_H as was demonstrated in experiments (see fig. S1) and simulations (fig. S2) for the fixed particle density ρ.

The change in the mean value of the local hexagonal bond-order parameter, $\langle|\psi_6|\rangle$, of the spinner lattices reveals a clear transition from the liquid to crystalline phase with increasing spinner density, ρ (Fig. 3C), which may be attributed to spinner confinement. At low ρ, the spinners can freely move around being advected by local hydrodynamic flows generated by the neighboring spinners, resulting in a liquid-like behavior. As the density of spinners increases, (e.g., ρ ≈ 0.0164 σ^{-2}), the spinners become more restricted in their motion due to hydrodynamic repulsive interaction from the neighbors and eventually become rather tightly confined, resulting in emergence of self-organized spinner lattices (Fig. 3A and movie S2).

The simulations yield a similar trend with the spinner density (see Fig. 4). As in the experiments, the average spacing between the spinners decreases together with the spinner size as ρ increases, and calculated streamlines (Fig. 4A) demonstrate gradual densifications of the vortices. Figure 4A also illustrates the presence of strong flow field inhomogeneities at low spinner densities that lead to spinners motion by advection. Gradual spinner density growth facilitates the confinement of the spinners and reduces these flow nonuniformities, leading to an overall stabilization of the spinner lattices with a characteristic of spinner-spinner spacing. The simulations capture the liquid-like order of the spinners at low densities, but the transition to a crystalline phase is not as pronounced as in the experiments. However, simulations of rod-like, fixed-length spinners with permanent bonds exhibit an order parameter dependence with increasing density similar to experiments (compare Figs. 4B and 3B). Hence, the experimentally obtained self-assembled spinners seem to be more stable than those emerging in simulations. We attribute the difference to a possible additional attraction of the Ni particles.

To further investigate and characterize the structural order of the dynamic spinner lattices in detail, we analyze the relative positions of the spinners within the ensemble. The spinners self-organize into lattices with a well-defined frequency-dependent interspinner spacing at high densities (e.g., ρ ~ 0.006 σ^{-2}; Fig. 5A). The presence of a short-range crystalline order in the dynamic lattices (see Fig. 5B) is manifested by pronounced peaks of the radial distribution function $g(r)$. As expected, these peaks shift toward smaller distances with increasing external field frequency f_H (the gray area in Fig. 5B). The trend is even better visualized by the behavior of the structure factor, $S(q)$

$$S(q) = 1 + 2\pi\rho\int_0^\infty [g(r) - 1]J_0(qr)\, rdr \qquad (3)$$

where q is the wave vector and $J_0(qr)$ is the zero-order Bessel function of the first kind (*44*). The lateral shift of the primary peak in the corresponding $S(q)$ curves toward larger q with increasing f_H is shown in Fig. 5C. Qualitatively, the same trend is obtained in simulations (see inset of Fig. 5C), although the shift in the peaks is less pronounced. The active spinner lattice contraction and expansion are fully reversible and could be remotely orchestrated on demand by tuning the frequency of the excitation field (Fig. 5D) and provide an in situ tuning of the active transport of cargo particles in the system.

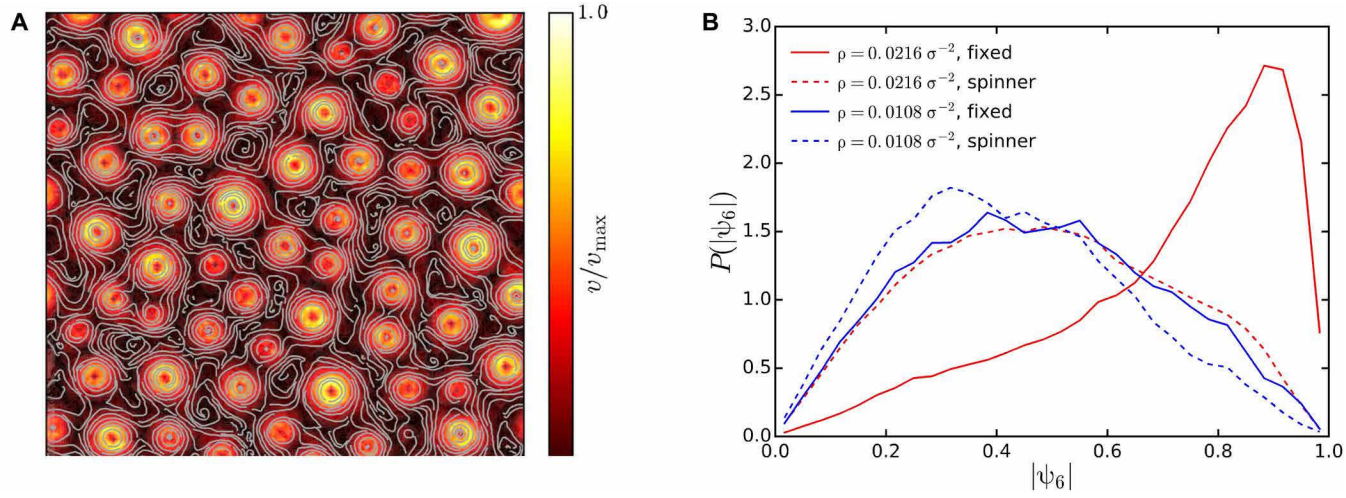

Fig. 4. Synchronized spinner ensemble in simulations. (**A**) Simulation snapshot of a spinner ensemble flow field formed at $\rho = 0.018\ \sigma^{-2}$ at frequency $\omega = 2\pi f_B = 0.05\ \tau^{-1}$. The nonuniform distribution of the spinner-spinner spacing induces strong flow field nonuniformities. (**B**) Probability distribution function of the hexagonal bond-orientational order parameter $|\psi_6|$ in the spinner lattices for self-assembled spinners (dashed lines) and spinners of fixed length and bonds (solid lines).

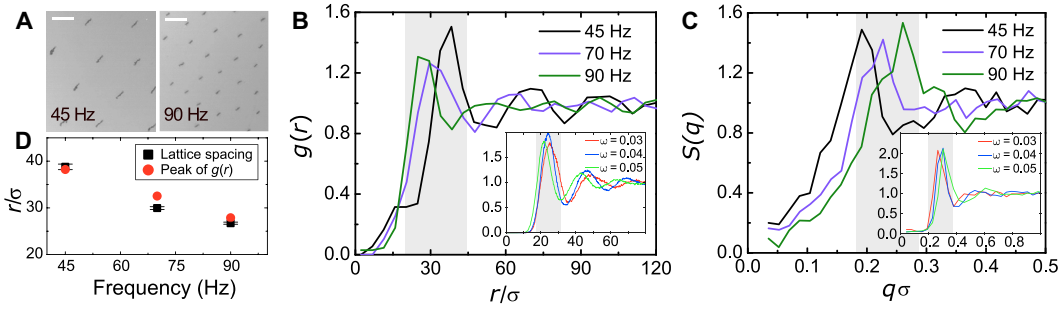

Fig. 5. Dynamic crystalline lattices of synchronized spinners. A dynamic lattice composed of (**A**) long spinners induced at $f_H = 45$ Hz and short spinners self-assembled at $f_H = 90$ Hz. The lattice formed at $f_H = 45$ Hz exhibits a larger interspinner spacing than the one formed at $f_H = 90$ Hz. Scale bars, 2 mm. (**B**) The radial distribution function and (**C**) the structure factor of the spinner lattices as a function of f_H from experimental results at $\rho = 0.006\ \sigma^{-2}$. Insets illustrate corresponding simulation results obtained at $\rho = 0.018\ \sigma^{-2}$. The gray area in (B) and (C) highlights the lateral shift of the primary peak with the frequency changes. (**D**) The experimental spinner-spinner distance at different frequencies as obtained from the Voronoi diagram analysis and $g(r)$ for data shown in (B).

Dynamics and transport inside the spinner lattices

The lattices of synchronized spinners give rise to a new class of active crystals accompanied by a vigorous vortical flow field (see movie S3). The system of synchronized spinners is intrinsically out of equilibrium, and the structure is maintained only while the continuous external energy input is present. Being active by nature, self-organized spinner lattices exhibit self-healing behavior. To demonstrate this property, we intentionally destroy locally the spinner lattice by means of a large glass bead (3 mm in diameter) passing through the interface (see Fig. 6 and movie S4). Once the bead is through the interface (Fig. 6B), the affected spot (Fig. 6C) is spontaneously self-repaired (Fig. 6D) within a few seconds. The self-healing process is driven by the emergence of strong flow inhomogeneities in the flow field between the disordered and ordered regions, which actively advect the spinners into the damaged region and restore the dynamic structure of the lattice. The lattice rupture and self-healing events are well reflected in the change of $\langle|\psi_6|\rangle$ (see Fig. 6E).

Because of the presence of strong self-induced underlying hydrodynamic flows (movie S3), a lattice of synchronized spinners is able to effectively facilitate transport of passive cargo particles (see the inset of Fig. 7A and movie S5). To characterize the activity-induced transport in the system, we determine the diffusion coefficient, D, for a passive nonmagnetic particle (~500 μm) placed inside a dynamic spinner lattice via tracking its mean square displacement (MSD). In both experiments and simulations, we observe the initial ballistic motion followed by a crossover to a diffusive regime, see Fig. 7, A and B, similar to the results observed in a bath of unsynchronized spinners (*38*). The diffusion coefficient D was then extracted from the linear part of the MSD curve, $\langle \Delta r^2 \rangle = 4D\Delta t$ (see Fig. 7A), with the particle displacement statistics well described by a Gaussian distribution (see fig. S3). We refer to the particle transport by a dynamic spinner lattice as an active diffusion, as the obtained D values in the range of 1 to 7 $mm^2\ s^{-1}$ are orders of magnitude higher than those corresponding to thermal Brownian diffusion for the same particle ($D_B = k_B T/(6\pi\nu R) \sim 8.6 \times 10^{-10}\ mm^2\ s^{-1}$, with Boltzmann constant k_B, temperature T, and particle radius R). A characteristic velocity scale for the ballistic motion can be estimated from the Stokes flow of Eq. 1. From Fig. 3, we obtain the typical spinner tracer distance $\bar{r} \approx 1$ mm at $f_H = 45$ Hz and the spinner length $L_S \approx 7 \times 90$ μm, which yields the velocity $v \approx 8$ mm/s in good agreement with the value of 6 mm/s extracted from the slope of Fig. 7.

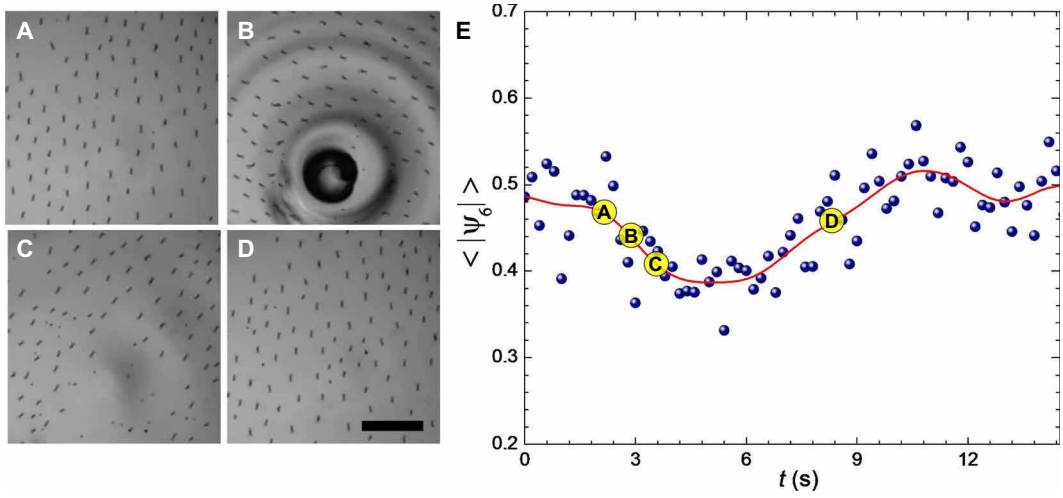

Fig. 6. Self-healing behavior in active spinner lattices. (**A** to **D**) Snapshots of a spinner lattice demonstrating the self-healing process: (A) A spinner lattice at $f_H = 90$ Hz, $\rho = 0.0112\,\sigma^{-2}$, (B) the moment of the lattice rapture by a 3-mm bead, (C) the lattice is locally fractured by the bead, and (D) spontaneously self-repaired lattice. Scale bar, 5 mm. (**E**) The time evolution of the mean bond orientational order parameter ψ_6 in the fractured region of the spinner lattice.

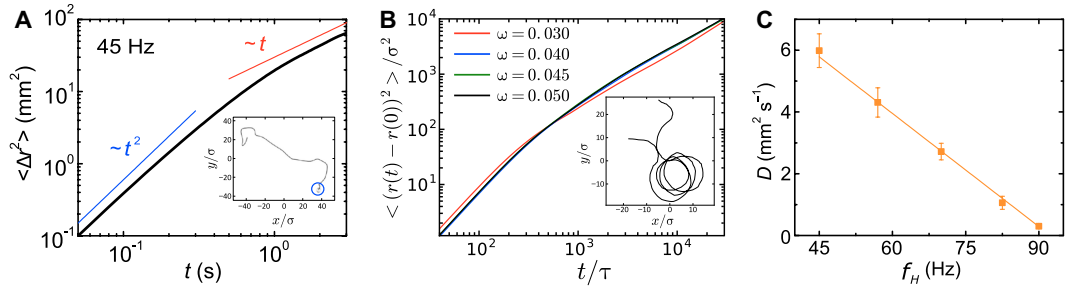

Fig. 7. Active transport in spinner lattices. (**A**) MSD of an inert particle of 500 μm diameter at $f_H = 45$ Hz. The blue and red lines represent the ballistic ($\propto\Delta t^2$) and normal diffusion regime ($\propto\Delta t$), respectively. Inset: A typical trajectory of the passive bead transported in the active spinner lattice. (**B**) MSD and an example trajectory of a transported passive particle as obtained in simulations for a passive particle of diameter σ at $\rho = 0.0108\,\sigma^{-2}$ (see movie S6). (**C**) Active diffusion coefficient as a function of the magnetic field frequency, f_H. The experiments were performed at $\rho = 0.006\,\sigma^{-2}$.

The active diffusion coefficient in active spinner material can be efficiently tuned by the parameters of the external energizing field. In Fig. 7C, we demonstrate that the value of the active diffusion coefficient for a large passive particle embedded in the spinner lattice can be substantially manipulated by the external field frequency. We observe an almost linear decrease of the active diffusion coefficient with the frequency increase. This behavior is attributed to the changes in the characteristic spinner-spinner distances within the lattice (see Fig. 5D), leading to a caging effect experienced by a cargo bead when a shrinkage of the spinner lattice unit cell coupled with the faster rotation of the spinners (faster induced flows) makes it more difficult for a passive particle to leave the cell.

As in experiments, simulations yield an enhanced tracer ballistic motion and diffusion for small and large tracer particles (σ and 5σ, respectively). However, the diffusion coefficient is essentially independent on the frequency f_H in all cases. For smaller size tracer particle, we attribute this effect to tracer confinement within the rotating field of a spinner for some time, often for several rotations, as is illustrated in Fig. 7B (see movie S6). In case of larger tracer and self-assembled spinners, their interaction with the spinner lattice leads to breakage of spinners and a (local) destruction of the spinner lattice. Hence, tracers diffuse essentially in the bare fluid and their long-time dynamics is little affected by the still, on larger scales, present spinner lattice. As concluded before, the spinners formed in experiments are more stable and less susceptible to perturbations by tracers than those in simulations. Stable lattices are obtained for systems of fixed-length spinners with permanent bonds for the frequency range $\omega\tau = 0.03$ to 0.05 and the monomer concentration $\rho = 0.018/\sigma^2$, where the spinner length is adjusted according to the frequency-dependent averages obtained for self-assembled spinners. Embedded large passive tracers of diameter 5σ exhibit an enhanced ballistic and diffusive motion (see movie S7). However, we do not observe a substantial frequency dependence for the diffusion coefficient as is obtained in experiments. Since the spinner lattice is hardly affected by the tracer, we attribute the obtained disagreement to differences in the hydrodynamic flow fields between the 3D experiments and the 2D simulations. Here, 3D simulations are required to clarify the origin of the observed discrepancy.

SUMMARY AND CONCLUSIONS

We report results of the structural and transport properties of a new active material composed of self-assembled synchronized spinners. Ferromagnetic microparticles suspended at an air-water interface

dynamically self-assemble into multiparticle spinners when energized by a rotating magnetic field applied in-plane of the interface. The activity in the system originates solely from the rotational motion of the spinners, in contrast to conventional active systems composed of self-propelling units. On the basis of experiments and simulations, we reveal that collective interactions between spinners give rise to new dynamic phases—spinner liquids and lattices. Self-organized spinner lattices support an active diffusion by means of vigorous self-generated hydrodynamic flows and are capable of self-healing behavior. The structural ordering and inherent dynamics of these out-of-equilibrium spinner lattices can be reversibly tuned by the parameters of the external excitation field. Comparison of 3D experimental and 2D simulation results suggests a fundamental dependence of the tracer transport on dimensionality of the flow field. We demonstrate that transport of inert cargo particles embedded in self-organized active spinner lattices can be remotely controlled and manipulated. These capabilities of synchronized spinner swarms open new opportunities in the design of self-assembled structures and tunable transport in active materials at the microscale.

MATERIALS AND METHODS

Experimental setup

Ferromagnetic Ni microparticles (Alfa Aesar) with an average diameter of 90 μm (75 to 106 μm uniform size distribution) were dispersed at the air-water interface in a cylindrical beaker (diameter, 5 cm; water depth, 4 cm). The Ni particles remained suspended at the interface supported by the surface tension of water throughout the experiments. The particles spontaneously formed self-assembled spinners when energized by an in-plane rotating magnetic field with amplitude (≈4 mT). Two sinusoidal signals with a π/2 phase shift were applied to two pairs of iron-core solenoids placed at an orthogonal angle and controlled by a computer. The container was housed on a microscope stage (Leica MZ9.5) where the dynamics of the particles was monitored by means of a fast complementary metal-oxide semiconductor camera (iNS1, Integrated Design Tools) at a frame rate of 50 to 500 frames/s.

A nonmagnetic glass bead with a diameter of 3 mm (GSM-30, Ceroglass Technologies Inc.) was used to investigate the self-healing process in the system. A nonmagnetic glass bead with a diameter of 500 μm (U-500, Novum Glass LLC) was used to determine the diffusion coefficient for active transport of a cargo particle in the system. Spherical gold powders (0.8 to 1.5 μm; Alfa Aesar) were used as tracers to visualize the self-induced hydrodynamic flows.

Data analysis

The image sequences were analyzed to investigate the structure and dynamics of the self-assembled spinner ensembles. Particle tracing was performed by a MATLAB script based on the Crocker and Grier algorithm (*45*) to identify the 2D location of each spinner. The *xy* coordinates of the spinners' centers were used to characterize the structural order in the systems: radial distribution function, structure factor, and bond-orientational order parameter. Particle image velocimetry (PIV) was used using MatPIV package to calculate the velocity field, vorticity field, and flow streamlines in the system.

Mesoscale simulations

Simulations are performed for 2D circular colloids embedded in an explicit fluid. A colloid consists of 18-point particles of mass M, which are uniformly distributed over the circumference of a circle of diameter σ, with an additional point particle at the center (*38*). The shape is maintained by strong harmonic bonds of suitable rest length, both between the nearest neighbors and each particle with the center. The harmonic bond potential is

$$U_{\text{bond}}(r) = \frac{K}{2}(r - r_0)^2 \tag{4}$$

where r is the distance between two point particles and r_0 is the preferred mean bond length. Each colloid carries a magnetic dipole. The interaction energy of a dipole with magnetic moment $\boldsymbol{\mu}$ and the rotating magnetic field $\boldsymbol{B}$ is

$$U_{\text{ext}} = -\boldsymbol{\mu} \cdot \boldsymbol{B} \tag{5}$$

The dipole-dipole interaction potential between two colloids at a distance R is

$$U_{\text{dipole}}\left(R\right) = -\frac{\mu_0}{4\pi R^3}\left[3\left(\boldsymbol{\mu_1} \cdot \hat{\boldsymbol{R}}\right)\left(\boldsymbol{\mu_2} \cdot \hat{\boldsymbol{R}}\right) - \boldsymbol{\mu_1} \cdot \boldsymbol{\mu_2}\right] \tag{6}$$

where μ_0 is the vacuum permeability, μ_1 and μ_1 are the respective magnetic moments, and $\hat{\boldsymbol{R}}$ is the unit vector along the center-to-center distance between the colloid pair. The colloid's excluded volume interaction is captured by the repulsive Lennard-Jones potential

$$U_{\text{LJ}} = 4\epsilon\left[\left(\frac{\sigma}{R}\right)^{24} - \left(\frac{\sigma}{R}\right)^{12} + \frac{1}{4}\right] \tag{7}$$

for $R < R_c$, where $R_c = \sqrt[12]{2}\,\sigma$ is the cutoff distance and ϵ is the interaction strength and U_{LJ} is zero otherwise. The dynamics of the colloids is treated by standard molecular dynamics simulations. To maintain the desired temperature, a local Maxwellian thermostat is applied (*46*).

The fluid is modeled by an angular momentum conserving variant (*37*, *47*, *48*) of the multiparticle collision (MPC) dynamics technique, a particle-based mesoscale simulation approach that accounts for hydrodynamic interactions (*49*). In MPC, lengths are scaled by the collision cell size a, mass by fluid mass m, and energy by k_BT; hence, the time unit is $\tau = \sqrt{ma^2/k_BT}$. The collision angle is set to $\alpha = 130^\circ$, and the collision time $h = 0.1\ \tau$. For this set of parameters, the 2D MPC fluid kinematic viscosity is $\nu = 0.37\ a^2/\tau$. The colloid diameter is $\sigma = 6a$, and the constituent point particle's mass $M = 10\ m$, which assures adequate fluid-colloid coupling in the MPC algorithm for the correct hydrodynamic behavior. The spring constant is $K = 5000\ k_BT/a^2$, large enough to maintain the circular shape. We use a time step of $\Delta t = 0.01\ \tau$ for the velocity Verlet integration of the Newton's equations of motion for the colloids. Then, simulations yield the colloid translational diffusion coefficient $D_0 = 4.4 \times 10^{-2}\ a^2/\tau$ and the rotational diffusion $D_R = 2 \times 10^{-3}\tau^{-1}$ in dilute solution. The colloids are subjected to the magnetic field $B_0 = 1.5\sqrt{k_B\,T\mu_0/a^3}$, and their magnetic moment is $\mu = 480\sqrt{k_B\,Ta^3}/\mu_0$. As in experiments, a rotating external magnetic field leads to self-assembled spinners of average length $L_s \approx 8\ \sigma$ at the frequency $f_B\tau = 0.008$.

SUPPLEMENTARY MATERIALS

Supplementary material for this article is available at http://advances.sciencemag.org/cgi/content/full/6/12/eaaz8535/DC1

Fig. S1. Experimentally obtained probability distribution of the hexagonal bond-orientational order parameter $|\psi_6|$ in the spinner lattices at $\rho = \sim 0.006\ \sigma^{-2}$ as a function of the field frequency.

Fig. S2. The probability distribution function of the hexagonal bond-orientational order parameter $|\psi_6|$ in the spinner lattices at $\rho = \sim 0.018\ \sigma^{-2}$ as obtained in simulations.

Fig. S3. Displacement statistics of passive cargo particles transported by a dynamic spinner lattices at $t = 1.5$ s.
Movie S1. Velocity, streamlines, and vorticity flow fields induced by synchronous spinners at a surface of water, as obtained in experiments.
Movie S2. A self-organized spinner lattice, as obtained in experiments.
Movie S3. A vigorous vortical flow field in a spinner crystal, as obtained in experiments.
Movie S4. Self-healing of a local order in a spinner ensemble.
Movie S5. Active transport of a 500-μm glass bead facilitated by a spinner lattice, as obtained in experiments.
Movie S6. Self-organized spinner lattice and active transport of a small tracer particle of diamter σ, as obtained in simulations.
Movie S7. Active transport of a large tracer particle of diamter 5σ in a lattice of fixed-length spinners, as obtained in simulations.

REFERENCES AND NOTES

1. G. M. Whitesides, B. Grzybowski, Self-assembly at all scales. *Science* **295**, 2418–2421 (2002).
2. W. Wang, W. Duan, S. Ahmed, A. Sen, T. E. Mallouk, From one to many: Dynamic assembly and collective behavior of self-propelled colloidal motors. *Acc. Chem. Res.* **48**, 1938–1946 (2015).
3. J. E. Martin, A. Snezhko, Driving self-assembly and emergent dynamics in colloidal suspensions by time-dependent magnetic fields. *Rep. Prog. Phys.* **76**, 126601 (2013).
4. K. Han, C. W. Shields IV, O. D. Velev, Engineering of self-propelling microbots and microdevices powered by magnetic and electric fields. *Adv. Funct. Mater.* **28**, 1705953 (2018).
5. A. Snezhko, I. S. Aranson, Magnetic manipulation of self-assembled colloidal asters. *Nat. Mater.* **10**, 698–703 (2011).
6. M. Driscoll, B. Delmotte, Leveraging collective effects in externally driven colloidal suspensions: Experiments and simulations. *Curr. Opin. Colloid Interface Sci.* **40**, 42–57 (2019).
7. K. J. Solis, J. E. Martin, Complex magnetic fields breathe life into fluids. *Soft Matter* **10**, 9136–9142 (2014).
8. A. Snezhko, I. Aranson, W.-K. Kwok, Surface wave assisted self-assembly of multidomain magnetic structures. *Phys. Rev. Lett.* **96**, 078701 (2006).
9. F. Martinez-Pedrero, P. Tierno, Magnetic propulsion of self-assembled colloidal carpets: Efficient cargo transport via a conveyor-belt effect. *Physical Review Applied* **3**, 051003 (2015).
10. A. Demortière, A. Snezhko, M. V. Sapozhnikov, N. Becker, T. Proslier, I. S. Aranson, Self-assembled tunable networks of sticky colloidal particles. *Nat. Commun.* **5**, 3117 (2014).
11. M. Guix, J. Orozco, M. García, W. Gao, S. Sattayasamitsathit, A. Merkoçi, A. Escarpa, J. Wang, Superhydrophobic alkanethiol-coated microsubmarines for effective removal of oil. *ACS Nano* **6**, 4445–4451 (2012).
12. J. Li, B. E.-F. de Ávila, W. Gao, L. Zhang, J. Wang, Micro/nanorobots for biomedicine: Delivery, surgery, sensing, and detoxification. *Sci. Robot* **2**, eaam6431 (2017).
13. C. Bechinger, R. Di Leonardo, H. Löwen, C. Reichhardt, G. Volpe, G. Volpe, Active particles in complex and crowded environments. *Rev. Mod. Phys.* **88**, 045006 (2016).
14. G. S. Redner, M. F. Hagan, A. Baskaran, Structure and dynamics of a phase-separating active colloidal fluid. *Phys. Rev. Lett.* **110**, 055701 (2013).
15. F. Martinez-Pedrero, E. Navarro-Argemí, A. Ortiz-Ambriz, I. Pagonabarraga, P. Tierno, Emergent hydrodynamic bound states between magnetically powered micropropellers. *Sci. Adv.* **4**, eaap9379 (2018).
16. H. H. Wensink, J. Dunkel, S. Heidenreich, K. Drescher, R. E. Goldstein, H. Löwen, J. M. Yeomans, Meso-scale turbulence in living fluids. *Proc. Natl. Acad. Sci. U.S.A.* **109**, 14308–14313 (2012).
17. A. Wysocki, R. G. Winkler, G. Gompper, Cooperative motion of active Brownian spheres in three-dimensional dense suspensions. *EPL* **105**, 48004 (2014).
18. A. Kaiser, A. Snezhko, I. S. Aranson, Flocking ferromagnetic colloids. *Sci. Adv.* **3**, e1601469 (2017).
19. M. Theers, E. Westphal, G. Gompper, R. G. Winkler, Modeling a spheroidal microswimmer and cooperative swimming in a narrow slit. *Soft Matter* **12**, 7372–7385 (2016).
20. M. Theers, E. Westphal, K. Qi, R. G. Winkler, G. Gompper, Clustering of microswimmers: Interplay of shape and hydrodynamics. *Soft Matter* **14**, 8590–8603 (2018).
21. B. A. Grzybowski, H. A. Stone, G. M. Whitesides, Dynamic self-assembly of magnetized, millimetre-sized objects rotating at a liquid–air interface. *Nature* **405**, 1033–1036 (2000).
22. S. Farhadi, S. Machaca, J. Aird, B. O. Torres Maldonado, S. Davis, P. E. Arratia, D. J. Durian, Dynamics and thermodynamics of air-driven active spinners. *Soft Matter* **14**, 5588–5594 (2018).
23. G. Kokot, D. Piet, G. M. Whitesides, I. S. Aranson, A. Snezhko, Emergence of reconfigurable wires and spinners via dynamic self-assembly. *Sci. Rep.* **5**, 9528 (2015).
24. C. Scholz, M. Engel, T. Pöschel, Rotating robots move collectively and self-organize. *Nat. Commun.* **9**, 931 (2018).
25. A. M. Brooks, M. Tasinkevych, S. Sabrina, D. Velegol, A. Sen, K. J. M. Bishop, Shape-directed rotation of homogeneous micromotors via catalytic self-electrophoresis. *Nat. Commun.* **10**, 495 (2019).
26. Z. Shen, A. Würger, J. S. Lintuvuori, Hydrodynamic self-assembly of active colloids: Chiral spinners and dynamic crystals. *Soft Matter* **15**, 1508–1521 (2019).
27. B. C. van Zuiden, J. Paulose, W. T. M. Irvine, D. Bartolo, V. Vitelli, Spatiotemporal order and emergent edge currents in active spinner materials. *Proc. Natl. Acad. Sci. U.S.A.* **113**, 12919–12924 (2016).
28. N. H. P. Nguyen, D. Klotsa, M. Engel, S. C. Glotzer, Emergent collective phenomena in a mixture of hard shapes through active rotation. *Phys. Rev. Lett.* **112**, 075701 (2014).
29. I. Llopis, I. Pagonabarraga, Hydrodynamic regimes of active rotators at fluid interfaces. *Eur. Phys. J. E* **26**, 103–113 (2008).
30. K. Yeo, E. Lushi, P. M. Vlahovska, Collective dynamics in a binary mixture of hydrodynamically coupled microrotors. *Phys. Rev. Lett.* **114**, 188301 (2015).
31. G. Kokot, A. Snezhko, Manipulation of emergent vortices in swarms of magnetic rollers. *Nat. Commun.* **9**, 2344 (2018).
32. A. Bricard, J.-B. Caussin, N. Desreumaux, O. Dauchot, D. Bartolo, Emergence of macroscopic directed motion in populations of motile colloids. *Nature* **503**, 95–98 (2013).
33. F. Ma, S. Wang, D. T. Wu, N. Wu, *Proc. Natl. Acad. Sci. U.S.A.* **112**, 6307–6312 (2015).
34. A. Snezhko, Complex collective dynamics of active torque-driven colloids at interfaces. *Curr. Opin. Colloid Interface Sci.* **21**, 65–75 (2016).
35. W. Wang, J. Giltinan, S. Zakharchenko, M. Sitti, Dynamic and programmable self-assembly of micro-rafts at the air-water interface. *Sci. Adv.* **3**, e1602522 (2017).
36. Y. Goto, H. Tanaka, Purely hydrodynamic ordering of rotating disks at a finite Reynolds number. *Nat. Commun.* **6**, 5994 (2015).
37. I. O. Götze, G. Gompper, Flow generation by rotating colloids in planar microchannels. *EPL* **92**, 64003 (2010).
38. G. Kokot, S. Das, R. G. Winkler, G. Gompper, I. S. Aranson, S. Alexey, Active turbulence in a gas of self-assembled spinners. *Proc. Natl. Acad. Sci. U.S.A.* **114**, 12870–12875 (2017).
39. Y. Gao, M. Hulsen, T. Kang, J. M. J. den Toonder, Numerical and experimental study of a rotating magnetic particle chain in a viscous fluid. *Phys. Rev. E* **86**, 041503 (2012).
40. N. Vogel, M. Retsch, C.-A. Fustin, A. del Campo, U. Jonas, Advances in colloidal assembly: The design of structure and hierarchy in two and three dimensions. *Chem. Rev.* **115**, 6265–6311 (2015).
41. I. Petousis, E. Homburg, R. Derks, A. Dietzel, *Lab Chip* **7**, 1746–1751 (2007).
42. E. Climent, K. Yeo, M. R. Maxey, G. E. Karniadakis, Dynamic self-assembly of spinning particles. *J. Fluids Eng.* **129**, 379–387 (2007).
43. W. Mickel, S. C. Kapfer, G. E. Schröder-Turk, K. Mecke, Shortcomings of the bond orientational order parameters for the analysis of disordered particulate matter. *J. Chem. Phys.* **138**, 044501 (2013).
44. A. Brodin, A. Nych, U. Ognysta, B. Lev, V. Nazarenko, M. Škarabot, I. Muševič, Melting of 2D liquid crystal colloidal structure. *Condens. Matter Phys.* **13**, 33601:1-12 (2010).
45. J. C. Crocker, D. G. Grier, Methods of digital video microscopy for colloidal studies. *J. Colloid Interface Sci.* **179**, 298–310 (1996).
46. C.-C. Huang, A. Chatterji, G. Sutmann, G. Gompper, R. G. Winkler, Cell-level canonical sampling by velocity scaling for multiparticle collision dynamics simulations. *J. Comput. Phys.* **229**, 168–177 (2010).
47. H. Noguchi, N. Kikuchi, G. Gompper, Particle-based mesoscale hydrodynamic techniques. *EPL* **78**, 10005 (2007).
48. M. Theers, R. G. Winkler, Effects of thermal fluctuations and fluid compressibility on hydrodynamic synchronization of microrotors at finite oscillatory Reynolds number: A multiparticle collision dynamics simulation study. *Soft Matter* **10**, 5894–5904 (2014).
49. G. Gompper, T. Ihle, D. M. Kroll, R. G. Winkler, Multi-Particle Collision Dynamics — A particle-based mesoscale simulation approach to the hydrodynamics of complex fluids. *Adv. Polym. Sci.* **221**, 1 (2009).

Acknowledgments
Funding: The research of K.H., G.K., and A.S. was supported by the U.S. Department of Energy, Office of Science, Basic Energy Sciences, Materials Sciences and Engineering Division. G.G. and R.G.W. acknowledge financial support from the Deutsche Forschungsgemeinschaft (DFG) within the priority program SPP 1726 "Microswimmers - From Single Particle Motion to Collective Behaviour." **Author contributions:** A.S. conceived the research. K.H., G.K., and A.S. performed the experiments and analysis of the experimental data. S.D., G.G. and R.G.W. conducted the numerical simulations. All authors wrote the manuscript. **Competing interests:** The authors declare that they have no competing interests. **Data and materials availability:** All data needed to evaluate the conclusions in the paper are present in the paper and/or the Supplementary Materials. Additional data related to this paper may be requested from the authors.

Submitted 14 October 2019
Accepted 31 December 2019
Published 20 March 2020
10.1126/sciadv.aaz8535

Citation: K. Han, G. Kokot, S. Das, R. G. Winkler, G. Gompper, A. Snezhko, Reconfigurable structure and tunable transport in synchronized active spinner materials. *Sci. Adv.* **6**, eaaz8535 (2020).

Reconfigurable structure and tunable transport in synchronized active spinner materials

Koohee Han, Gasper Kokot, Shibananda Das, Roland G. Winkler, Gerhard Gompper and Alexey Snezhko

Sci Adv **6** (12), eaaz8535.
DOI: 10.1126/sciadv.aaz8535